
Multi-level Multiple Instance Learning with Transformer for Whole Slide Image Classification

Ruijie Zhang¹ Qiaozhe Zhang¹ Yingzhuang Liu¹ Hao Xin²
 Yan Liu² Xinggang Wang^{1*}

¹Huazhong University of Science and Technology ²Ant Group
 {k1seki, qiaozhezhang, xgwang}@hust.edu.cn

Abstract

Whole slide image (WSI) refers to a type of high-resolution scanned tissue image, which is extensively employed in computer-assisted diagnosis (CAD). The extremely high resolution and limited availability of region-level annotations make it challenging to employ deep learning methods for WSI-based digital diagnosis. Multiple instance learning (MIL) is a powerful tool to address the weak annotation problem, while Transformer has shown great success in the field of visual tasks. The combination of both should provide new insights for deep learning based image diagnosis. However, due to the limitations of single-level MIL and the attention mechanism's constraints on sequence length, directly applying Transformer to WSI-based MIL tasks is not practical. To tackle this issue, we propose a Multi-level MIL with Transformer (MMIL-Transformer) approach. By introducing a hierarchical structure to MIL, this approach enables efficient handling of MIL tasks that involve a large number of instances. To validate its effectiveness, we conducted a set of experiments on WSIs classification task, where MMIL-Transformer demonstrate superior performance compared to existing state-of-the-art methods. Our proposed approach achieves test AUC 94.74% and test accuracy 93.41% on CAMELYON16 dataset, test AUC 99.04% and test accuracy 94.37% on TCGA-NSCLC dataset, respectively. All code and pre-trained models are available at: <https://github.com/hustvl/MMIL-Transformer>

1 Introduction

Deep learning's success [16; 17; 29; 38; 43; 32] in sequential image tasks offers promising methods for digital pathology. Whole slide images (WSIs), which are high-resolution digital slides of tissue specimens, are commonly used in image-based digital pathology [15]. However, the huge size and absence of pixel/region-level annotations [31] in WSIs create obstacles for deep learning-based image diagnosis. To address the aforementioned problem, image-based computer-assisted diagnostics typically employ multiple instance learning (MIL) [21; 8], a subset of weakly supervised learning methods [44].

The dataset of a MIL task is organized into multiple bags, with each bag consisting of multiple instances. The annotations are only available at the bag level. This data organization offers significant benefits in the field of image-based digital pathology. For instance, in cancer diagnosis, the entire WSI (bag-level data) can be labeled as tumor without the necessity of distinguishing normal tissue (instances) within the WSI. This approach substantially alleviates the challenges associated with data and annotations acquisition. However, challenges persist due to the high resolution of WSI and the unbalanced distribution of instance categories.

*Xinggang Wang is the corresponding author

Previous studies have explored the applications of MIL in digital pathology tasks. [39; 20] perform pooling operation on instance feature embeddings then to following tasks. [18] introduce attention mechanism, where trainable attention weights are given to each instance for aggregation. Li et al. [24] introduced non-local attention to MIL, where the similarity is measured between the instance to give distinct attention weights. To introduce correlated information between instances, [30] uses Nyström Attention [40] based transformer to calculate global attention between all instances in one bag.

Transformer [36] adopts the self-attention mechanism, which calculates the pairwise correlation between each token within a sequence. Self-attention mechanism enables Transformer to effectively capture both the spatial morphology features of individual patches, as well as the correlation information between different patches [5]. However, when working with high-resolution WSIs, Transformer would yield a prohibitively large number of patches, making it challenging to use the original self-attention mechanism. To address this problem, one approach is to use approximate attention [40; 3], but may not capture all the intricate relationships within the sequence compared to the original self-attention mechanism. Another approach is to perform local-attention [19; 26], which can be classified into two strategies. The first strategy is a non-overlapped approach, reducing computational complexity to a great extent but lacking the capability to capture global information. The second strategy is overlapped approach, which enhances communication among local elements. Nonetheless, as the sequence length grows, this strategy introduces supplementary computational complexity [10].

In response to the aforementioned challenges, inspired by the MSG-Transformer [10], we propose the Multi-level MIL with Transformer (MMIL-Transformer) method, a hierarchical MIL framework with Transformer. The MMIL-Transformer utilizes non-approximate self-attention and incorporates local-attention for processing long sequences of WSI. Of particular significance is the introduction of a hierarchical MIL framework shown in Fig. 1, where multiple-level bags are generated from the original WSI. Multiple-head self-attention (MSA) is performed only within each sub-bag with messenger (*MSG*) tokens and these *MSG* tokens are treated as higher-level bag data for the following operations. MMIL is a hierarchical learning strategy for large-scale multi-instance learning, i.e., the size of input instances is large. It solves the contradiction between the need for Transformer for accurate MIL and the high computation cost of Transformer with large-scale instances.

To demonstrate its effectiveness, we evaluate MMIL-Transformer on two public WSI datasets, i.e., CAMELYON16 [2] and TCGA-NSCLC [34]. The proposed model achieved a promising test AUC 94.74% and test accuracy 93.41% on CAMELYON16 dataset, test AUC 99.04% and test accuracy 94.37% on TCGA-NSCLC dataset. We expect our efforts can further ease the research and application of Transformers for large-scale MIL.

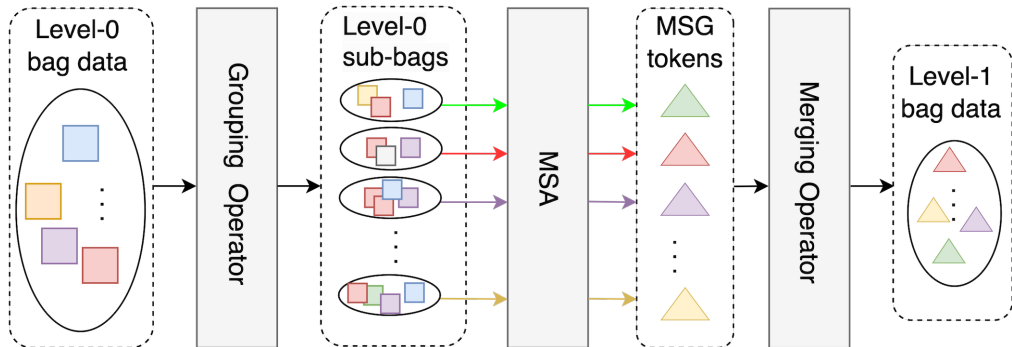


Figure 1: A two-level Multiple Instance Learning framework. 1) A level-0 bag is divided into several sub-bags by a grouping operator; 2) Perform a messenger-based MSA to obtain *MSG* tokens; 3) Merge all *MSG* tokens by a merging operator to build level-1 bag data, all *MSG* tokens after merging are treated as instances of level-1 bag; 4) Hierarchical bags can be generated by repeating 1), 2) and 3).

2 Related Work

2.1 Whole Slide Images Pre-processing

WSI scanners are capable of converting biopsy slide tissue into a gigapixel image by capturing the image in small, overlapping sections and stitching them together to form a high-resolution image of the entire slide, typically at $20\times$ to $40\times$ magnification. These images fully preserve the original tissue structure, which is crucial for computer-assisted diagnostics (CAD) [15]. To read or manipulate WSI, there are several open-source tools available, such as OpenSlides [11] and QuPath [1]. However, due to the presence of a large number of background images and noise images in WSI, it is necessary to perform corresponding processes on them. There are two main categories of methods for WSI processing. The first one is a classic image processing method, where the clipped WSI patches are converted to the HSV color space, and then subjected to background removal and denoising based on hue, Saturation and value [33]. The second category is a deep learning based method [27; 24], where a classifier like CNN is trained to distinguish whether the clipped patches are tissue or not.

2.2 Multiple Instance Learning in Pathology

Keeler et al [21] first proposed Multiple Instances Learning, which is especially useful for tasks where the data is presented as a set of instances, and the label is only given to the whole set. In the pathology field, MIL methods can be categorized into two types, instance-based MIL [20; 4; 41; 23; 6] and embedding-based MIL [27; 30; 24], based on the input data for aggregation module. Instance-based MIL methods first map extracted patches to pseudo-labels that correspond to the bag-level annotation, and then use these corresponding top-k instances for aggregation. Due to the unbalanced distribution of different instance types, instance-based methods always require a large number of WSIs. Embedding-based MIL methods first map extracted patches to embeddings then feed all patch feature embeddings to the following modules. Recently, attention mechanism have gained interest in MIL. [18; 35; 13; 28; 27] introduce trainable weights to each instance. To further improve the performance, non-local attention [24] and self-attention [30] is also adopted in MIL. Most previous MIL methods focused on evaluating the labels of instances, [39] emphasizes the representation of bags.

2.3 Self-attention Mechanism

The inception of Transformer [36] can be traced back to the domain of natural language processing (NLP), where the self-attention mechanism plays a pivotal role in establishing relations between local features. ViT [9] is the first model to extend Transformers to vision tasks, where a plain Transformer is applied to patch sequences clipped from images. For gigapixel images, the patch sequence becomes too long to process in self-attention mechanism. Local-attention and approximate-attention can be employed to address this problem. [3] introduce a fixed-size sliding window to sequences, MSA is only performed within the windows. [7] propose sparse-Transformer, where a subset of the input sequence is selected by adaptive mechanisms to calculate self-attention. [37] introduce a low-rank factorization of the attention matrix. There are also other local-attention methods [22; 42]. However, local-attention methods present a trade-off dilemma where non-overlapped windows lack communication between each window, while overlapped windows make more computational burden as the sequence goes longer. And the adoption of approximate attention in models results in information loss, reducing the interpretability of the model. Therefore, we require a more efficient, simple, and flexible approach to building local-global relations to handle high-resolution images like WSIs. [10] proposed a messenger mechanism to the non-overlapped window attention method, which enables the information exchange between separated windows.

Motivated by the messenger mechanism proposed in [10], we incorporate this mechanism into MIL to establish a hierarchical framework. However, We do not treat *MSG* tokens only as a hub for communication between fixed windows like in [10]. These tokens are actually higher-level instances of the original bag. Thus, we further make use of these *MSG* tokens to build higher-level bags and demonstrate its effectiveness in extremely high-resolution MIL tasks.

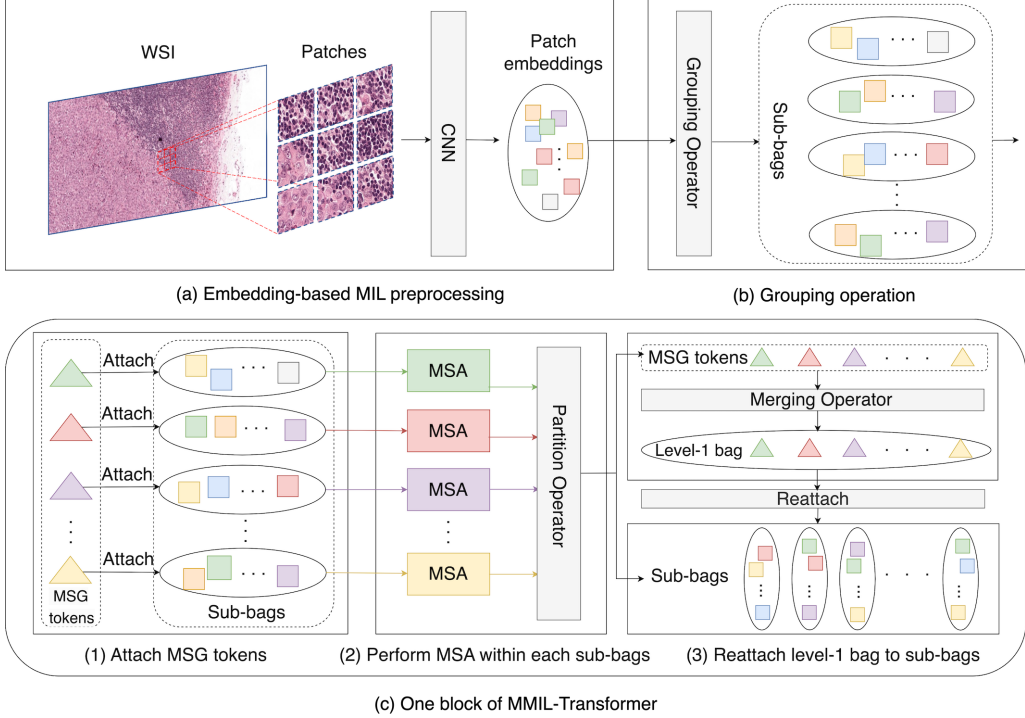


Figure 2: Overview of a two-level MMIL-Transformer. (a) WSI Pre-processing: 1) Background removal; 2) Clip tissue images into patches; 3) Mapping patches to feature embeddings. (b) Grouping operation: split feature embeddings into sub-bags. (c) One block of MMIL-Transformer: (1) Attach *MSG* tokens to each sub-bag. (2) Perform MSA within each sub-bag then part sub-bags from *MSG* tokens; 3) Merge Parted *MSG* tokens to build a level-1 bag, then reattach all tokens in level-1 bag to level-0 sub-bags;

3 Method

3.1 Transformer-based Multiple Instance Learning

MIL Problem Formulation In MIL, given N bag-level samples $\{\mathbf{X}_1, \mathbf{X}_2, \dots, \mathbf{X}_N\}$ and their corresponding bag-level label $\{\mathbf{Y}_1, \mathbf{Y}_2, \dots, \mathbf{Y}_N\}$, each bag-level data \mathbf{X}_i is made of numbers of instances $\{\mathbf{x}_{i,1}, \mathbf{x}_{i,2}, \dots, \mathbf{x}_{i,n_i}\}$, where the instance-level labels $\{\mathbf{y}_{i,1}, \mathbf{y}_{i,2}, \dots, \mathbf{y}_{i,n_i}\}$ are unknown. Suppose we have a model denoted by $f(\theta)$, a binary MIL classification task is to give bag-level prediction $\hat{\mathbf{Y}}_i = f(\mathbf{X}_i; \theta) \in \{0, 1\}$ as close to the bag-level label $\mathbf{Y}_i \in \{0, 1\}$ as possible, i.e., $\arg \min_{\theta} L(\hat{\mathbf{Y}}_i, \mathbf{Y}_i)$, where L denotes the loss function and n_i is the number of instances of i -st bag-level data. The MIL constraints are illustrated as follows.

$$\mathbf{Y}_i = \begin{cases} x = 0, \text{ iff } \sum \mathbf{y}_{i,j} = 0 & \mathbf{y}_{i,j} \in \{0, 1\} \quad j = 1 \dots n_i \\ y = 1, \text{ otherwise} \end{cases} \quad (1)$$

Apply Transformer to MIL-based WSIs Classification In the context of a Transformer-based binary classification problem on WSIs, we define bag-level data as referring to WSIs, where label 0 denotes normal WSI and label 1 denotes WSI containing tumors. Leveraging the Transformer mechanism, we segment the WSI into patches of size $P \times P$ (e.g., 256×256) to serve as instances. These patches are then passed through a Transformer and a decoder to obtain the classification results. To reduce computational complexity, we can employ an embedding-based approach, where we initially feed segmented patches to a feature extractor (e.g., ResNet[14]) and use the resulting feature sequences as input to the Transformer. Due to the gigapixel of WSI, the resulting feature sequences are too long to perform MSA. Therefore, we propose a multi-level MIL framework for applying Transformer.

3.2 Build Multi-level Bags for WSI

In this section, we demonstrate how to build hierarchical bags for WSI. The construction process involves two primary stages, aiming at building a higher-level bag from its corresponding lower-level counterpart. The first stage is grouping, where the lower bag is first divided into sub-bags by a grouping operator. In the second stage, a messenger-based MSA is performed within each sub-bag. MSG tokens are then used to produce a higher-level bag through a merging operator.

Grouping Operators The utilization of grouping operators allows us to partition lengthy sequences into shorter sub-bags, thus enabling performing MSA. We instantiated types of grouping operators. Each of these operators possesses its own set of pros and cons.

- *Coordinate grouping*: we employ the original coordinates of patches as the basis for grouping. Specifically, we preserve the central coordinates of all clipped patches from a WSI when pre-processing, and use these coordinates for K-Means [12] clustering. Sub-bags are created by the index of clustering results.
- *Embedding grouping*: we use the cosine distance between embeddings for clustering, then treat the result as sub-bags. This approach does not require additional coordinate information.
- *Random grouping*: we randomly group the embeddings to specific numbers of sub-bags. The index remains the same during training.
- *Sequential grouping*: the embeddings are grouped into numbers of sub-bags in sequential order, with the original patches arranged on the WSI from left to right and top to bottom.

Coordinate grouping introduces additional information into sub-bags, which may potentially enhance performance. Embedding grouping does not require an additional step in pre-processing, but the lack of spatial information will impact the performance. These clustering-based grouping methods incur higher computational resource costs. Random grouping is simple, and it may bring a benefit for unbalanced data problems. Additionally, grouping operators can be designed freely for different requirements.

Corresponding with grouping operators, we further introduce a *masking mechanism* to speed up the model and enhance its performance. Specifically, after partitioning sequences into sub-bags, a fixed ratio of the sub-bags will be masked. These masked sub-bags will be deposed for the following processing.

Messenger Mechanism We introduce the messenger mechanism [10] to exchange local information between sub-bags and use all MSG tokens to produce higher-level bags. As shown in Fig. 2(c), m MSG tokens $T_{MSG}^j \in \mathbb{R}^{m \times C}$ will be attached to each sub-bag $G_j \in \mathbb{R}^{w_j \times C}$ as $G_j' \in \mathbb{R}^{(w_j+m) \times C}$, where C denotes the embedding channel of patch feature, w_j denotes the number of members in j -th sub-bag. Therefore, one WSI is divided into MSG token attached sub-bags $\{G_1', G_2', \dots, G_g'\}$. MSA is performed within each sub-bag between both feature embeddings and MSG tokens. MSG tokens can capture information from the corresponding sub-bag with attention. Finally, all MSG tokens from different sub-bags are collected and undergo a merging operation to produce a higher-level bag. Moreover, a class(CLS) token is attached to the higher-level bag for the classification task. Actually, this CLS token can be regarded as the final-level bag.

Merging Operation There are many merge operations used in [10], including but not limited to shuffle and average. However, these operations appear to be ill-suited for application within the current context. Therefore, we further introduce self-attention to MSG tokens. After performing MSA with patch embeddings, the patch embeddings are partitioned from the MSG tokens and the MSG tokens are subsequently fed into a Transformer.

Overall, the process to generate multi-level bags for WSI can be summarized as Alg. 1.

3.3 MMIL-Transformer

We now present MMIL-Transfomer. As shown in Fig. 2, we first preprocess WSI following the procedure mentioned in Fig. 2(a), which converts high-resolution WSI to patch embeddings. These embeddings are fed into MMIL-Transfomer layers. In one basic layer, higher-level bags are generated

Algorithm 1: Bulid k -level bags for WSI

Input: Bag-level data \mathbf{X}_h^0
Output: Set of k level bags \mathbf{X}_h^K
for each level **do**
 1) Grouping and masking \mathbf{X}_h^l to g sub-bags by grouping operation c ;
 $\{G_1, G_2, \dots, G_g\} \leftarrow c(\mathbf{X}_h^l)$, where $G_j \in \mathbb{R}^{w_j \times C}$, $\sum w_j = n$, $j \in \{1, 2, \dots, g\}$;
 2) Attach MSG tokens to each sub-bags;
 $G_j' \leftarrow \text{Concat}(T_{MSG}^j; G_j)$, $j \in \{1, 2, \dots, g\}$;
 3) Perform MSA in each sub-bag;
 $G_j' \leftarrow \text{MSA}(G_j') + G_j'$;
 4) Merging all MSG tokens to build higher level bag;
 $\mathbf{X}_h^{l+1} \leftarrow \text{Merge}(T_{MSG}^1, T_{MSG}^2, \dots, T_{MSG}^g)$
 5) Append \mathbf{X}_h^{l+1} to \mathbf{X}_h^K .
end for
6) Attach CLS token to highest level bag;
 $\mathbf{X}_h^K \leftarrow \text{Concat}(\mathbf{X}_h^K, T_{cls})$
return \mathbf{X}_h^K

through Alg. 1. MSA is performed within every-level sub-bags, lower-level sub-bags communicate with each other through a merging operation. It is worth noting that the higher-level bags are derived from the MSG tokens obtained from lower-level sub-bags. This relationship allows for their reattachment to the corresponding lower-level sub-bags, thereby enabling the implementation of a multi-layer design for MMIL-Transformer. Finally, the model will give a prediction to one WSI by performing MLP to the class token T_{cls} . We summarize the whole MMIL-Transformer as Alg. 2.

Complexity Analysis For a sequence $S \in \mathbb{R}^{p \times C}$, where p is the length of S , C is number of channels. The complexity of the original MSA per layer is $\mathcal{O}(p^2 \times C)$. Assuming we divide S into g sub-bags evenly as the result $G \in \mathbb{R}^{g \times \frac{p}{g} \times C}$. The complexity of MSA per sub-bag is $\mathcal{O}((\frac{p}{g})^2 \times C)$. Thus, for one specific level bag, the total complexity of MSA per layer in MMIL-Transformer is $\mathcal{O}(\frac{1}{g} \times p^2 \times C)$.

Algorithm 2: MMIL-Transformer

Input: Bag of instances $\mathbf{X}_i = \{x_{i,1}, x_{i,2}, \dots, x_{i,n}\}$ from one WSI
Output: Bag-level prediction $\hat{\mathbf{Y}}_i$
for each layer **do**
 1) Embed the instances to feature space by h ;
 $\mathbf{X}_h \leftarrow h(\mathbf{X}_i)$, where $\mathbf{X}_h \in \mathbb{R}^{n \times C}$;
 2) Build k -level bags \mathbf{X}_h^K by Alg. 1, denoted by MLB;
 $X_h^K = \text{MLB}(\mathbf{X}_h)$, where $X_h^K = \{X_h^0, X_h^1, \dots, X_h^k\}$;
 3) Reattach X_h^{l+1} to X_h^l for all $X_h^l \in X_i^K$;
 $X_h^l = \text{Concat}(X_h^{l+1}, X_h^l)$, for $l \in \{0, 1, \dots, k\}$;
 4) Fed X_h^0 to next layer;
end for
5) Give prediction $\hat{\mathbf{Y}}$ though T_{cls} ;
 $\hat{\mathbf{Y}} \leftarrow \text{MLP}(T_{cls})$
return $\hat{\mathbf{Y}}$

4 Experiments

To demonstrate the superior performance of the proposed MMIL-Transformer, we conducted various experiments on the CAMELYON16 [2] dataset and TCGA-NSCLC [34] dataset.

Dataset and Evaluation Metrics CAMELYON16 is a public dataset for metastasis detection in hematoxylin and eosin (H&E) stained WSIs of lymph node sections. The dataset contains 270 training WSIs and 129 test WSIs. We perform pre-processing at $\times 20$ magnification, which produces 4.6 million 256×256 non-overlapping patches. All patches are mapped to feature embeddings by ImageNet pre-trained ResNet50 [14] baseline.

The TCGA-NSCLC dataset focuses on non-small cell lung cancer (NSCLC), encompassing two types of carcinoma: Lung Squamous Cell Carcinoma (TCGA-LUSC) and Lung Adenocarcinoma (TCGA-LUAD). TCGA-NSCLC comprises a total of 1053 diagnostic WSIs, with 541 slides from 478 cases for LUAD and 512 slides from 478 cases for LUSC. For pre-processing, we adopt the same configuration as DSMIL [24], where a total of 1046 WSIs are involved in the computation. We split the dataset in the ratio of training:validation:test = 60:15:25, resulting in 627 training WSIs, 156 validation WSIs and 263 test WSIs.

To evaluate the classification performance, we utilized accuracy and area under the curve (AUC) scores as the evaluation metrics. In all experiments, the accuracy was calculated using a fixed threshold of 0.5.

Experiments Details We employ cross-entropy as our loss function, and the Adma optimizer was employed with a learning rate of 1e-4 and weight decay of 1e-5. The default number of basic layers is 2. For the CAMELYON16 dataset, we grouped the embeddings into 10 sub-bags using the *random grouping* operator and randomly masked the sub-bags by a ratio of 0.6. As for the TCGA-NSCLC dataset, we employed *random grouping* to split the embeddings into 4 sub-bags. In both datasets, one single *MSG* token is attached to each sub-bag. These *MSG* tokens are then used to construct higher-level bags structure for later modules. All experiments were conducted using a 24GB RTX 3090 GPU.

4.1 Results on WSI Classification

The binary classification tasks encompass the identification of positive and negative cases within the CAMELYON16 dataset, LUSC and LUAD subtypes within the TCGA-NSCLC dataset. All results are presented in Tab. 1. Compared with other state-of-the-art methods [30; 27; 24; 4; 18; 25], the proposed MMIL-Transformer consistently achieves superior results in both accuracy and AUC score on both datasets. Note that all test experiments are conducted 10 times in test datasets to calculate the average accuracy and AUC.

Table 1: Results on CAMELYON16 and TCGA-NSCLC

Method	Publication	CAMELYON16		TCGA-NSCLC	
		Accuracy	AUC	Accuracy	AUC
ABMIL[18]	ICML 2018	0.8682	0.8760	0.7719	0.8656
PT-MTA[25]	MICCAI 2019	0.8217	0.8454	0.7379	0.8299
MIL-RNN[4]	Nature Med 2019	0.8450	0.8880	0.8619	0.9107
DSMIL[24]	CVPR 2021	0.7985	0.8179	0.8058	0.8925
CLAM-SB[27]	Nature BME 2021	0.8760	0.8809	0.8180	0.8818
CLAM-MB[27]	Nature BME 2021	0.8372	0.8679	0.8422	0.9377
TransMIL[30]	NeurIPS 2021	0.8837	0.9309	0.8835	0.9603
MMIL-Transformer	-	0.9341	0.9474	0.9437	0.9904

The CAMELYON16 dataset exhibits an imbalanced distribution of normal tissue patches and tumor tissue patches, posing significant challenges for the classification task. However, MMIL-Transformer overcomes these challenges and achieves a notable improvement of 5.04% accuracy and 1.65% AUC compared to the TransMIL. CLAM, PT-MTA, and ABMIL do not consider the correlation between instances, which leads to limited performance. In comparison to other non-attention methods, the utilization of clustering operation in CLAM has enabled it to achieve relatively better performance.

In the TCGA-NSCLC dataset, there is a higher abundance of positive tissue patches compared to negatives, resulting in relatively easier identification of LUSC with LUAD. All mentioned methods achieve relatively better performance than their performance on CAMELYON16. However, MMIL-

Transformer stands out with an impressive accuracy of 94.37%, which is at least 6% higher than the other methods. Furthermore, MMIL-Transformer achieves promising results on test AUC score of 99.04%.

4.2 Ablation Study

We further conducted a series of ablation studies to determine the contribution of several proposed modules.

4.2.1 Effects of Grouping Operator

To determine the impact of different grouping operators, we performed a series of experiments while keeping the other configurations unchanged. Notably, to avoid the effects of randomness, we employ *coordinate grouping* instead of *random grouping* on CAMELYON16, *embedding grouping* instead of *random grouping* on TCGA-NSCLC.

We first study the influence of the number of sub-bags. The results are shown in Tab. 2. In CAMELYON16 the test AUC decays as the number of sub-bags increases. This behavior can be attributed to the trade-off between the number of sub-bags and available memory resources. Larger numbers of sub-bags require less memory and computational cost, but it makes obstacles to effective communication between them. It can be predicted that the accuracy will be lower as the number of sub-bags increases. In TCGA-NSCLC, there are relatively fewer patches (with a minimum of 23 patches) in WSIs, we were able to split the dataset into up to 6 sub-bags using clustering. Compared with CAMELYON16, the performance deterioration in TCGA-NSCLC is relatively minor.

Table 2: Effects of Different Grouping Numbers.

Dataset	Sub-bags number	Accuracy	AUC
CAMELYON16	10	0.8992	0.9500
	16	0.8682	0.9305
	32	0.8992	0.9314
	64	0.8837	0.8816
TCGA-NSCLC	2	0.9354	0.9896
	4	0.9392	0.9887
	6	0.9316	0.9890

We also studied the effect of different grouping methods, the experiment was conducted on CAMELYON16, and the results are shown in Tab. 3. An interesting observation is that the incorporation of additional coordinate information leads to a performance decline in terms of accuracy. In our view, the utilization of random grouping alleviates the influence of instance imbalance. Through the process of random grouping, each sub-bag has the potential to be allocated positive instances. This enables the attention mechanism to focus on the positive instances within each sub-bag, thereby enhancing the accuracy of the model. Conversely, the incorporation of positional information may give rise to a substantial quantity of sub-bags that lack positive instances, thereby exacerbating the issue of imbalance on higher-level bags. On the other hand, embedding grouping, which does not need additional information, yields relatively lower accuracy and AUC scores. When we group the embeddings in sequential order, thereby utilizing ill spatial information, the resulting scores in accuracy and AUC are lower.

Table 3: Effects of Different Grouping Methods.

Dataset	Method	Accuracy	AUC
CAMELYON16	Coordinate grouping	0.8992	0.9500
	Embedding grouping	0.8682	0.9216
	Sequential grouping	0.8604	0.9097
	Random grouping	0.9178	0.9419

4.2.2 Effects of Masking

We conducted several experiments to determine the effects of the masking mechanism. The grouping method is *random grouping* on two datasets. The results are presented in Tab.4. In the case of the CAMELYON16 datasets, the inclusion of the masking mechanism results in a 1.63% enhancement to the performance. However, for relatively more balanced datasets TCGA-NSCLC, the masking mechanism has minimal impact on its performance while demanding significantly lower training resources.

Table 4: Effects of Different Masking Mechanism.

Dataset	Sub-bags number	Masking ration	Accuracy	AUC
CAMELYON16	10	0.6	0.9341	0.9474
		0.3	0.9302	0.9372
		0	0.9178	0.9419
TCGA-NSCLC	4	0.25	0.9391	0.9901
		0.75	0.9395	0.9902
		0	0.9437	0.9904

4.2.3 Effects of Multi-level Framework

In CAMELYON16, patches of different WSIs in $\times 20$ magnification range from 142 to 55852. In TCGA-NSCLC, patches range from 23 to 14990. The minimum number of patches determines the maximum number of sub-bags that can be formed, consequently limiting the dimension of higher-level bags. Thus, A two-level structure is enough for both datasets. Ablation experiments are conducted on CAMELYON16 by using *coordinate grouping* for the reason of its relative more patches. Again, due to the impracticality of directly performing MSA on level-0 bags as the sequences are too long, we conduct this part experiments by using a Nyström Attention method for fairness. The results are shown in Tab. 5. MMIL-Transformer achieves a similar result as TransMIL in 0-level bags due to they both employ an approximate-attention. The performance on level-1 is much worse than level-0 due to the trade-off mentioned in 4.2.1 and the information loss from approximate-attention. This multi-level framework enables the proposed model to perform non-approximate MSA, which achieves much better performance.

Table 5: Effects of Multi-level Framework.

Dataset	k	Accuracy	AUC	Approximate-attention
CAMELYON16	0	0.8759	0.9227	✓
	1	0.6667	0.6650	✓
	1	0.8992	0.9500	✗

5 Discussion and Conclusion

In our work, we have proposed a multi-level MIL framework with Transformer method for long-sequence MIL tasks. The proposed model first splits bag-level data into sub-bags, by introducing messenger mechanism to each sub-bags, it can build hierarchical bags for less computational cost of non-approximate MSA. Benefiting from non-approximate MSA mechanism and its multi-level framework, MMIL-Transformer can better establish local-global connections with less complexity, which makes it more suitable for unbalanced/balanced MIL classification. MMIT-Transformer outperforms the state-of-the-art MIL methods in terms of both AUC and accuracy over public datasets.

Limitations and Future Work When dealing with CAMELYON16, we find the performance is more sensitive to the grouping results due to the unbalanced problem. There should be a more suitable grouping operator for making the performance more stable. We will explore these issues in the follow-up work.

References

- [1] Peter Bankhead, Maurice B Loughrey, José A Fernández, Yvonne Dombrowski, Darragh G McArt, Philip D Dunne, Stephen McQuaid, Ronan T Gray, Liam J Murray, Helen G Coleman, et al. Qupath: Open source software for digital pathology image analysis. *Scientific reports*, 7(1):1–7, 2017.
- [2] Babak Ehteshami Bejnordi, Mitko Veta, Paul Johannes Van Diest, Bram Van Ginneken, Nico Karssemeijer, Geert Litjens, Jeroen AWM Van Der Laak, Meyke Hermsen, Quirine F Manson, Maschenka Balkenhol, et al. Diagnostic assessment of deep learning algorithms for detection of lymph node metastases in women with breast cancer. *Jama*, 318(22):2199–2210, 2017.
- [3] Iz Beltagy, Matthew E Peters, and Arman Cohan. Longformer: The long-document transformer. *arXiv preprint arXiv:2004.05150*, 2020.
- [4] Gabriele Campanella, Matthew G Hanna, Luke Geneslaw, Allen Miraflor, Vitor Werneck Krauss Silva, Klaus J Busam, Edi Brogi, Victor E Reuter, David S Klimstra, and Thomas J Fuchs. Clinical-grade computational pathology using weakly supervised deep learning on whole slide images. *Nature medicine*, 25(8):1301–1309, 2019.
- [5] Jieneng Chen, Yongyi Lu, Qihang Yu, Xiangde Luo, Ehsan Adeli, Yan Wang, Le Lu, Alan L Yuille, and Yuyin Zhou. Transunet: Transformers make strong encoders for medical image segmentation. *arXiv preprint arXiv:2102.04306*, 2021.
- [6] Philip Chikontwe, Meejeong Kim, Soo Jeong Nam, Heounjeong Go, and Sang Hyun Park. Multiple instance learning with center embeddings for histopathology classification. In *Medical Image Computing and Computer Assisted Intervention–MICCAI 2020: 23rd International Conference, Lima, Peru, October 4–8, 2020, Proceedings, Part V 23*, pages 519–528. Springer, 2020.
- [7] Rewon Child, Scott Gray, Alec Radford, and Ilya Sutskever. Generating long sequences with sparse transformers. *arXiv preprint arXiv:1904.10509*, 2019.
- [8] Thomas G Dietterich, Richard H Lathrop, and Tomás Lozano-Pérez. Solving the multiple instance problem with axis-parallel rectangles. *Artificial intelligence*, 89(1-2):31–71, 1997.
- [9] Alexey Dosovitskiy, Lucas Beyer, Alexander Kolesnikov, Dirk Weissenborn, Xiaohua Zhai, Thomas Unterthiner, Mostafa Dehghani, Matthias Minderer, Georg Heigold, Sylvain Gelly, et al. An image is worth 16x16 words: Transformers for image recognition at scale. *arXiv preprint arXiv:2010.11929*, 2020.
- [10] Jiemin Fang, Lingxi Xie, Xinggang Wang, Xiaopeng Zhang, Wenyu Liu, and Qi Tian. Msg-transformer: Exchanging local spatial information by manipulating messenger tokens. In *Proceedings of the IEEE/CVF Conference on Computer Vision and Pattern Recognition*, pages 12063–12072, 2022.
- [11] Adam Goode, Benjamin Gilbert, Jan Harkes, Drazen Jukic, and Mahadev Satyanarayanan. Openslide: A vendor-neutral software foundation for digital pathology. *Journal of pathology informatics*, 4(1):27, 2013.
- [12] John A Hartigan and Manchek A Wong. Algorithm as 136: A k-means clustering algorithm. *Journal of the royal statistical society. series c (applied statistics)*, 28(1):100–108, 1979.
- [13] Noriaki Hashimoto, Daisuke Fukushima, Ryoichi Koga, Yusuke Takagi, Kaho Ko, Kei Kohno, Masato Nakaguro, Shigeo Nakamura, Hidekata Hontani, and Ichiro Takeuchi. Multi-scale domain-adversarial multiple-instance cnn for cancer subtype classification with unannotated histopathological images. In *Proceedings of the IEEE/CVF conference on computer vision and pattern recognition*, pages 3852–3861, 2020.
- [14] Kaiming He, Xiangyu Zhang, Shaoqing Ren, and Jian Sun. Deep residual learning for image recognition. In *Proceedings of the IEEE conference on computer vision and pattern recognition*, pages 770–778, 2016.

- [15] Lei He, L Rodney Long, Sameer Antani, and George R Thoma. Histology image analysis for carcinoma detection and grading. *Computer methods and programs in biomedicine*, 107(3):538–556, 2012.
- [16] Han Hu, Zheng Zhang, Zhenda Xie, and Stephen Lin. Local relation networks for image recognition. In *Proceedings of the IEEE/CVF International Conference on Computer Vision*, pages 3464–3473, 2019.
- [17] Zilong Huang, Xinggang Wang, Lichao Huang, Chang Huang, Yunchao Wei, and Wenyu Liu. Ccnet: Criss-cross attention for semantic segmentation. In *Proceedings of the IEEE/CVF international conference on computer vision*, pages 603–612, 2019.
- [18] Maximilian Ilse, Jakub Tomczak, and Max Welling. Attention-based deep multiple instance learning. In *International conference on machine learning*, pages 2127–2136. PMLR, 2018.
- [19] Max Jaderberg, Karen Simonyan, Andrew Zisserman, et al. Spatial transformer networks. *Advances in neural information processing systems*, 28, 2015.
- [20] Fahdi Kanavati, Gouji Toyokawa, Seiya Momosaki, Michael Rambeau, Yuka Kozuma, Fumihiro Shoji, Koji Yamazaki, Sadanori Takeo, Osamu Iizuka, and Masayuki Tsuneki. Weakly-supervised learning for lung carcinoma classification using deep learning. *Scientific reports*, 10(1):9297, 2020.
- [21] James Keeler, David Rumelhart, and Wee Leow. Integrated segmentation and recognition of hand-printed numerals. *Advances in neural information processing systems*, 3, 1990.
- [22] Nikita Kitaev, Łukasz Kaiser, and Anselm Levskaya. Reformer: The efficient transformer. *arXiv preprint arXiv:2001.04451*, 2020.
- [23] Marvin Lerousseau, Maria Vakalopoulou, Marion Classe, Julien Adam, Enzo Battistella, Alexandre Carré, Théo Estienne, Théophraste Henry, Eric Deutsch, and Nikos Paragios. Weakly supervised multiple instance learning histopathological tumor segmentation. In *Medical Image Computing and Computer Assisted Intervention–MICCAI 2020: 23rd International Conference, Lima, Peru, October 4–8, 2020, Proceedings, Part V 23*, pages 470–479. Springer, 2020.
- [24] Bin Li, Yin Li, and Kevin W Eliceiri. Dual-stream multiple instance learning network for whole slide image classification with self-supervised contrastive learning. In *Proceedings of the IEEE/CVF conference on computer vision and pattern recognition*, pages 14318–14328, 2021.
- [25] Weijian Li, Viet-Duy Nguyen, Haofu Liao, Matt Wilder, Ke Cheng, and Jiebo Luo. Patch transformer for multi-tagging whole slide histopathology images. In *Medical Image Computing and Computer Assisted Intervention–MICCAI 2019: 22nd International Conference, Shenzhen, China, October 13–17, 2019, Proceedings, Part I 22*, pages 532–540. Springer, 2019.
- [26] Ze Liu, Yutong Lin, Yue Cao, Han Hu, Yixuan Wei, Zheng Zhang, Stephen Lin, and Baining Guo. Swin transformer: Hierarchical vision transformer using shifted windows. In *Proceedings of the IEEE/CVF international conference on computer vision*, pages 10012–10022, 2021.
- [27] Ming Y Lu, Drew FK Williamson, Tiffany Y Chen, Richard J Chen, Matteo Barbieri, and Faisal Mahmood. Data-efficient and weakly supervised computational pathology on whole-slide images. *Nature biomedical engineering*, 5(6):555–570, 2021.
- [28] Nikhil Naik, Ali Madani, Andre Esteva, Nitish Shirish Keskar, Michael F Press, Daniel Ruderman, David B Agus, and Richard Socher. Deep learning-enabled breast cancer hormonal receptor status determination from base-level h&e stains. *Nature communications*, 11(1):5727, 2020.
- [29] Prajit Ramachandran, Niki Parmar, Ashish Vaswani, Irwan Bello, Anselm Levskaya, and Jon Shlens. Stand-alone self-attention in vision models. *Advances in neural information processing systems*, 32.
- [30] Zhuchen Shao, Hao Bian, Yang Chen, Yifeng Wang, Jian Zhang, Xiangyang Ji, et al. Transmil: Transformer based correlated multiple instance learning for whole slide image classification. *Advances in neural information processing systems*, 34:2136–2147, 2021.

- [31] Chetan L Srinidhi, Ozan Ciga, and Anne L Martel. Deep neural network models for computational histopathology: A survey. *Medical Image Analysis*, 67:101813, 2021.
- [32] Mingxing Tan and Quoc Le. Efficientnet: Rethinking model scaling for convolutional neural networks. In *International conference on machine learning*, pages 6105–6114. PMLR, 2019.
- [33] Ye Tian, Li Yang, Wei Wang, Jing Zhang, Qing Tang, Mili Ji, Yang Yu, Yu Li, Hong Yang, and Airong Qian. Computer-aided detection of squamous carcinoma of the cervix in whole slide images. *arXiv preprint arXiv:1905.10959*, 2019.
- [34] Katarzyna Tomczak, Patrycja Czerwińska, and Maciej Wiznerowicz. Review the cancer genome atlas (tcga): an immeasurable source of knowledge. *Contemporary Oncology/Współczesna Onkologia*, 2015(1):68–77, 2015.
- [35] Naofumi Tomita, Behnaz Abdollahi, Jason Wei, Bing Ren, Arief Suriawinata, and Saeed Hassانpour. Attention-based deep neural networks for detection of cancerous and precancerous esophagus tissue on histopathological slides. *JAMA network open*, 2(11):e1914645–e1914645, 2019.
- [36] Ashish Vaswani, Noam Shazeer, Niki Parmar, Jakob Uszkoreit, Llion Jones, Aidan N Gomez, Łukasz Kaiser, and Illia Polosukhin. Attention is all you need. *Advances in neural information processing systems*, 30, 2017.
- [37] Sinong Wang, Belinda Z Li, Madian Khabsa, Han Fang, and Hao Ma. Linformer: Self-attention with linear complexity. *arXiv preprint arXiv:2006.04768*, 2020.
- [38] Xiaolong Wang, Ross Girshick, Abhinav Gupta, and Kaiming He. Non-local neural networks. In *Proceedings of the IEEE conference on computer vision and pattern recognition*, pages 7794–7803, 2018.
- [39] Xinggang Wang, Yongluan Yan, Peng Tang, Xiang Bai, and Wenyu Liu. Revisiting multiple instance neural networks. *Pattern Recognition*, 74:15–24, 2018.
- [40] Yunyang Xiong, Zhanpeng Zeng, Rudrasis Chakraborty, Mingxing Tan, Glenn Fung, Yin Li, and Vikas Singh. Nyströmformer: A nyström-based algorithm for approximating self-attention. In *Proceedings of the AAAI Conference on Artificial Intelligence*, volume 35, pages 14138–14148, 2021.
- [41] Gang Xu, Zhigang Song, Zhuo Sun, Calvin Ku, Zhe Yang, Cancheng Liu, Shuhao Wang, Jianpeng Ma, and Wei Xu. Camel: A weakly supervised learning framework for histopathology image segmentation. In *Proceedings of the IEEE/CVF International Conference on computer vision*, pages 10682–10691, 2019.
- [42] Manzil Zaheer, Guru Guruganesh, Kumar Avinava Dubey, Joshua Ainslie, Chris Alberti, Santiago Ontanon, Philip Pham, Anirudh Ravula, Qifan Wang, Li Yang, et al. Big bird: Transformers for longer sequences. *Advances in neural information processing systems*, 33:17283–17297, 2020.
- [43] Hengshuang Zhao, Jiaya Jia, and Vladlen Koltun. Exploring self-attention for image recognition. In *Proceedings of the IEEE/CVF conference on computer vision and pattern recognition*, pages 10076–10085, 2020.
- [44] Zhi-Hua Zhou. A brief introduction to weakly supervised learning. *National science review*, 5(1):44–53, 2018.